Temporal optical memory based on coherent population and two-photon coherence oscillations

Asaf Eilam and A. D. Wilson-Gordon
Department of Chemistry, Bar-Ilan University, Ramat Gan 5290002, Israel

(Received 7 February 2018; published 5 July 2018)

We consider the $F_g = 1 \rightarrow F_e = 1$ transition between the ground and excited hyperfine levels in alkali-metal vapor interacting with σ linearly polarized control and probe fields whose polarizations can be either parallel or perpendicular to each other. We develop a matrix formulation that allows a solution of the Bloch equations to all orders in the pump and probe Rabi frequencies. Using this formalism, we calculate the steady-state probe absorption spectrum, the coherent population oscillations (CPOs), and two-photon coherence, in the absence (degenerate case) and presence (nondegenerate case) of a longitudinal magnetic field. We then calculate the probe storage when the pump is switched off and on again. We are particularly interested in whether the probe regains its original temporal shape when the pump is switched on again for the case of identical pump and probe frequencies. We show that, in the nondegenerate case, the restored probe does not regain its original shape whereas, in the degenerate case, the original shape is restored. This can be explained by considering the relative magnitudes of the CPOs which do not remember the temporal shape of the probe and the two-photon coherence oscillations which store the probe shape when the pump is switched off, as in electromagnetically induced transparency memories. In the nondegenerate case, the CPOs are much stronger than the two-photon coherence oscillations whereas, in the degenerate case, they are of similar magnitudes. Thus it is the two-photon coherence oscillations that are responsible for the restoration of the temporal shape of the probe in the degenerate case.

DOI: 10.1103/PhysRevA.98.013808

I. INTRODUCTION

Optical memories based on quantum processes are of great importance as they are essential elements in communication networks [1]. Our theoretical work on the storage of light via coherent population oscillations (CPOs) [2] has recently attracted experimental interest and such storage has been demonstrated in atomic systems at room temperature [3,4]. CPO occurs when two coherent electromagnetic fields interact with the same two-level transition. If the weaker probe field is detuned slightly from the stronger control field, the populations of the ground and excited states oscillate at the pump-probe frequency difference. CPO can lead to sharp dips (transparency windows) or peaks in the probe absorption spectrum when the pump and probe frequencies coincide [5–10]. For example, a dip (transparency window) appears in the probe absorption spectrum of a simple two-level system (TLS) when the transverse decay rate is much greater than the longitudinal decay rate as in the case of a saturable absorber [6,11]; in this case, the minimum width is equal to the decay rate of the excited state. In an open TLS, a sharp dip occurs in the probe absorption spectrum [9,10] [and a peak in the four-wave mixing (FWM) spectrum [12]] when the decay of the lower-energy state is smaller than the decay out of the system of the higher-energy state. The width of the sharp dip is determined by the decay due to the time of flight of the atoms through the laser beams, which can be reduced by either introducing a buffer gas into the cell or coating the cell with a paraffin coating. In common with dips due to electromagnetically induced transparency (EIT), the CPO dips are associated with a positive slope of the dispersion curve which leads to slowing down of the group velocity of the light on propagation [12].

A CPO dip also occurs when the TLS decays through a cascade of one or more intermediate states [5]. For the case of a single metastable state, the minimum width of the CPO dip is equal to the decay rate of the metastable level [5,8,13] which can be very small, so that the CPO can live a long time. We have studied this system in a variety of contexts [2,8,13,14]; in particular, we showed that it could be used to construct a spatial optical memory [2]. Unlike storage in EIT systems, where the temporal shape of the stored pulse is restored [15], CPO-based storage in a TLS with a metastable shelving state results in distortion of the temporal shape of the restored pulse [2].

This was also found to be the case in CPO-based light-storage *experiments* performed on metastable He [3,16] and Cs [4] atomic vapor where the pump and signal fields have orthogonal linear polarizations and a longitudinal magnetic field leads to Zeeman splitting of the ground and excited states. However, storage of orbital angular momentum has been demonstrated in both CPO-based [17,18] and EIT-based [19,20] experiments in cold Cs atoms.

In this paper (see Fig. 1), we consider the $F_g = 1 \rightarrow F_e = 1$ transition between the ground and excited hyperfine levels in alkali-metal vapor interacting with σ linearly polarized pump and probe in the absence or presence of a longitudinal magnetic field and solve both the Bloch and Maxwell-Bloch equations. In particular, we discuss light storage in this system. Our primary motivation in exploring this system is to determine whether the temporal shape of the probe can be restored and under which conditions. This question has not been investigated in previous work on this system. In our earlier work on a TLS that decays via a metastable state [2], we showed that the *temporal* shape of the probe pulse could *not* be restored although it was possible to restore its spatial shape. We were

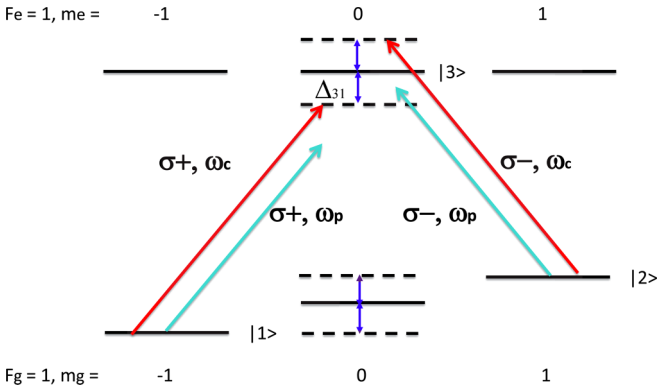

FIG. 1. Energy-level scheme for $F_g = 1 \rightarrow F_e = 1$ transition in the presence of longitudinal magnetic field interacting with σ polarized control (red) and probe (green) fields. The control frequency ω_c is resonant with the $F_g = 1, m_g = 0 \rightarrow F_e = 1, m_e = 0$ transition and the probe can have a polarization which is parallel or perpendicular to that of the control.

intrigued to find out whether these conclusions were also valid for other systems.

In Fig. 1, the $F_g = 1, m_g = -1 \rightarrow F_e = 1, m_e = 0$ transition interacts with the σ_+ component of the control and probe fields with frequencies ω_c and ω_p, whereas the $F_g = 1, m_g = 1 \rightarrow F_e = 1, m_e = 0$ transition interacts with the σ_- component of the control and probe fields. The transition-dipole moments of these transitions are equal and the control frequency ω_c is resonant with the $F_g = 1, m_g = 0 \rightarrow F_e = 1, m_e = 0$ transition frequency. For simplicity, we will label the $F_g = 1, m_g = -1$ and $F_g = 1, m_g = 1$ Rabi sublevels as $|1\rangle$ and $|2\rangle$, respectively, and the $F_e = 1, m_e = 0$ sublevel as $|3\rangle$. These three levels constitute a Λ system since spontaneous decay from the excited state $F_e = 1, m_e = 0$ to the Raman sublevel of the ground state $F_g = 1, m_g = 0$ is forbidden and we will treat the system here as if it is a Λ system. In the absence of a longitudinal magnetic field, the lower states $|1\rangle$ and $|2\rangle$ are degenerate and therefore in resonance with the pump field, whereas in the presence of such a field, the lower states are symmetrically detuned with respect to the pump field. Both these situations are studied for two configurations of the pump and probe polarizations: parallel (lin $\parallel$ lin) and perpendicular (lin $\perp$ lin).

In order to solve the Bloch equations, we adopt a matrix formalism that has been developed specifically for the system shown in Fig. 1 and is valid even for intense probes (for very weak probes, the formalism developed in [21] can also be used). Using the Floquet expansion to all orders in the pump and probe Rabi frequencies, we write the time-dependent Bloch equations in a computationally convenient tridiagonal matrix form and calculate the probe absorption spectrum, the coherent population oscillations of the lower states, and the two-photon coherence oscillations, as a function of δ. We also show that fields are created at the four-wave mixing (FWM) frequencies in the presence of the pump and probe fields. A study of the behavior of these quantities is essential in order to determine the factors that influence the storage of a probe pulse in this system.

We then solve the Maxwell-Bloch equations in order to study the storage of a probe pulse and the generated FWM pulse as a resonant pump is switched off and on. We stress that, to our knowledge, these equations have not been solved before for this system. We find that the temporal shape of the probe is only restored in the degenerate case whereas, in the nondegenerate case, the restored probe suffers from temporal distortion. We show that both the population and coherence oscillations of the ground Zeeman sublevels play a role in storing the probe but it is the coherence oscillations rather than the population oscillations that are responsible for the restoration of the probe's temporal shape. It should be noted that, while storage of the temporal pulse shape cannot be achieved by CPO alone, one can still obtain storage of its spatial shape in the same way as for the TLS that decays via a metastable state [2]. Some aspects of this study, such as propagation in a thick medium of a nonperturbative probe, have previously been explored by Pack *et al.* in a single Λ system under EIT conditions [22].

II. EQUATIONS OF MOTION

The time evolution of the density-matrix elements of the Λ system of Fig. 1 interacting with a control field of frequency ω_c and probe field of frequency ω_p is given by [23,24]

$$\dot{\rho}_{11} = iV_{13}\rho'_{31} - iV_{31}\rho'_{13} - \gamma_t\left(\rho_{11} - \rho_{11}^{eq}\right) + \Gamma_{31}\rho_{33}, \quad (1)$$

$$\dot{\rho}_{22} = iV_{23}\rho'_{32} - iV_{32}\rho'_{23} - \gamma_t\left(\rho_{22} - \rho_{22}^{eq}\right) + \Gamma_{32}\rho_{33}, \quad (2)$$

$$\dot{\rho}_{33} = -iV_{13}\rho'_{31} + iV_{31}\rho'_{13} - iV_{23}\rho'_{32} + iV_{32}\rho'_{23} - (\Gamma_{31} + \Gamma_{32} + \gamma_{3t})\rho_{33}, \quad (3)$$

$$\dot{\rho}'_{21} = iV_{23}\rho'_{31} - iV_{31}\rho'_{23} - i(\Delta_{21} - i\gamma_{21})\rho'_{21}, \quad (4)$$

$$\dot{\rho}'_{31} = iV_{31}(\rho_{11} - \rho_{33}) + iV_{32}\rho'_{21} - i(\Delta_{31} - i\gamma_{31})\rho'_{31}, \quad (5)$$

$$\dot{\rho}'_{32} = iV_{32}(\rho_{22} - \rho_{33}) + iV_{31}\rho'_{12} - i(\Delta_{32} - i\gamma_{32})\rho'_{32}, \quad (6)$$

$$\dot{\rho}_{ij} = \dot{\rho}^*_{ji}, \quad (7)$$

where

$$V_{31} = V_{13}^* = V_c + V_p e^{i\delta t},$$
$$V_{32} = V_{23}^* = V_c + rV_p e^{i\delta t}, \quad (8)$$

with $V_c = i\mu E_c/2\sqrt{2}\hbar$ for a σ_y polarized pump, $V_p = i\mu E_p/2\sqrt{2}\hbar$ and $r = +1$ for a σ_y polarized probe, and $V_p = -\mu E_p/2\sqrt{2}\hbar$ and $r = -1$ for a σ_x polarized probe [25], $\mu = \mu_{31} = \mu_{32}$, and

$$\rho'_{31,32} = \rho_{31,32}e^{-i\Delta_{31,32}t},$$
$$\rho'_{21} = \rho_{21}e^{-i\Delta_{21}t}, \quad (9)$$

with $\delta = \omega_c - \omega_p$, $\Delta_{31,32} = \omega_{31,32} - \omega_c$, and $\Delta_{21} = \omega_{21} = \Delta_{31} - \Delta_{32}$. The terms Γ_{ij} are the rates of decay of population from level $i \rightarrow j$, $\Gamma_3 = \Gamma_{31} + \Gamma_{32}$, γ_t is the rate of transfer to and from the reservoir, and $\gamma_{3t} - \gamma_t$ is the rate of decay of the upper level out of the system when the system is open (as in

a noncycling atomic transition). The decay rates of the optical coherences are given by $\gamma_{31} = \gamma_{32} = \frac{1}{2}(\Gamma_3 + \gamma_{3t} + \gamma_t) + \gamma^*$, where γ^* is the rate of decay due to phase-changing collisions (taken to be zero in the calculations). The decay rate of the Raman coherences is $\gamma_{21} = \gamma_{12} = \gamma_t$.

We now substitute the Floquet expansion

$$\rho = \sum_{n=-\infty}^{n=\infty} \rho^{(n)} e^{in\delta t} \tag{10}$$

in Eqs. (1)–(7) and express the resulting equations in matrix form as

$$\rho = -i\mathbf{A}\rho + \mathbf{B}, \tag{11}$$

where ρ is a column matrix with $9(2n_{\max}+1)$ elements, where $n_{\max}$ is the maximum value of n. For each value of n, there are nine elements given by

$$\rho^{(n)} = \begin{pmatrix} \rho_{11}^{(n)} \\ \rho_{22}^{(n)} \\ \rho_{33}^{(n)} \\ \rho_{21}^{\prime(n)} \\ \rho_{12}^{\prime(n)} \\ \rho_{31}^{\prime(n)} \\ \rho_{13}^{\prime(n)} \\ \rho_{32}^{\prime(n)} \\ \rho_{23}^{\prime(n)} \end{pmatrix}. \tag{12}$$

All the elements of $\mathbf{B}$ are zero except for the $(9n_{\max}+1, 9n_{\max}+2)$th terms, which are $\gamma_t \rho_{11,22}^{eq}$. $\mathbf{A}$ is a tridiagonal matrix of the form

$$\mathbf{A} = \begin{pmatrix} \mathbf{D}^{(-\mathbf{n}_{\max})} & \mathbf{R} & 0 & \cdots & 0 \\ \mathbf{L} & \mathbf{D}^{(-n_{\max}+1)} & \mathbf{R} & & \vdots \\ 0 & \ddots & \ddots & \ddots & 0 \\ \vdots & & \mathbf{L} & \mathbf{D}^{(n_{\max}-1)} & \mathbf{R} \\ 0 & \cdots & 0 & \mathbf{L} & \mathbf{D}^{(n_{\max})} \end{pmatrix}, \tag{13}$$

where $\mathbf{L}$, $\mathbf{D}^n$, $\mathbf{R}$ are given by

$$\mathbf{L} = \begin{pmatrix} 0 & 0 & 0 & 0 & 0 & 0 & V_p & 0 & 0 \\ 0 & 0 & 0 & 0 & 0 & 0 & 0 & 0 & rV_p \\ 0 & 0 & 0 & 0 & 0 & 0 & -V_p & 0 & -rV_p \\ 0 & 0 & 0 & 0 & 0 & 0 & 0 & 0 & V_p \\ 0 & 0 & 0 & 0 & 0 & 0 & rV_p & 0 & 0 \\ -V_p & 0 & V_p & -rV_p & 0 & 0 & 0 & 0 & 0 \\ 0 & 0 & 0 & 0 & 0 & 0 & 0 & 0 & 0 \\ 0 & -rV_p & rV_p & 0 & -V_p & 0 & 0 & 0 & 0 \\ 0 & 0 & 0 & 0 & 0 & 0 & 0 & 0 & 0 \end{pmatrix}, \tag{14}$$

$$\mathbf{D}^{(n)} = \begin{pmatrix} f_{11}^{(n)} & 0 & i\Gamma_{31} & 0 & 0 & -V_c^* & V_c & 0 & 0 \\ 0 & f_{22}^{(n)} & i\Gamma_{32} & 0 & 0 & 0 & 0 & -V_c^* & V_c \\ 0 & 0 & f_{33}^{(n)} & 0 & 0 & V_c^* & -V_c & V_c^* & -V_c \\ 0 & 0 & 0 & f_{21}^{(n)} & 0 & -V_c^* & 0 & 0 & V_c \\ 0 & 0 & 0 & 0 & f_{12}^{(n)} & 0 & V_c & -V_c^* & 0 \\ -V_c & 0 & V_c & -V_c & 0 & f_{31}^{(n)} & 0 & 0 & 0 \\ V_c^* & 0 & -V_c^* & 0 & V_c^* & 0 & f_{13}^{(n)} & 0 & 0 \\ 0 & -V_c & V_c & 0 & -V_c & 0 & 0 & f_{32}^{(n)} & 0 \\ 0 & V_c^* & -V_c^* & V_c^* & 0 & 0 & 0 & 0 & f_{23}^{(n)} \end{pmatrix}, \tag{15}$$

$$\mathbf{R} = \begin{pmatrix} 0 & 0 & 0 & 0 & 0 & -V_p^* & 0 & 0 & 0 \\ 0 & 0 & 0 & 0 & 0 & 0 & 0 & -rV_p^* & 0 \\ 0 & 0 & 0 & 0 & 0 & V_p^* & 0 & rV_p^* & 0 \\ 0 & 0 & 0 & 0 & 0 & -rV_p^* & 0 & 0 & 0 \\ 0 & 0 & 0 & 0 & 0 & 0 & 0 & -V_p^* & 0 \\ 0 & 0 & 0 & 0 & 0 & 0 & 0 & 0 & 0 \\ V_p^* & 0 & -V_p^* & 0 & rV_p^* & 0 & 0 & 0 & 0 \\ 0 & 0 & 0 & 0 & 0 & 0 & 0 & 0 & 0 \\ 0 & rV_p^* & -rV_p^* & V_p^* & 0 & 0 & 0 & 0 & 0 \end{pmatrix}, \tag{16}$$

and $f_{11}^{(n)} = f_{22}^{(n)} = n\delta - i\gamma_t$, $f_{33}^{(n)} = n\delta - i\Gamma_3 - i\gamma_{3t}$, $f_{21}^{(n)} = \Delta_{21} + n\delta - i\gamma_{21}$, $f_{12}^{(n)} = -\Delta_{21} + n\delta - i\gamma_{21}$, $f_{31,32}^{(n)} = \Delta_{31,32} + n\delta - i\gamma_{31,32}$, and $f_{13,23}^{(n)} = -\Delta_{31,32} + n\delta - i\gamma_{31,32}$.

We consider the case where the pump and probe propagate along the z direction, the pump is σ_y linearly polarized, and the probe has either the same polarization as the pump (lin ∥ lin) as in [24], or is perpendicularly polarized (σ_x, lin ⊥ lin) with respect to the pump as in [3,4], and substitute the appropriate values of V_p and r in the probe absorption, which is proportional to $\mathrm{Im}(\rho_{31}'^{(1)}/V_p + \rho_{32}'^{(1)}/rV_p)$ [26].

The main purpose of this paper is to investigate when it is possible to restore the probe pulse's temporal shape after storage. In order to calculate the probe propagation, we solve the propagation equations for a control field with time dependence

$$V_c(t,z=0) = V_c(t=0,z=0)\{(1-0.5\tanh[\Gamma(t-\tau_1)] + 0.5\tanh[\Gamma(t-\tau_2)]\}, \quad (17)$$

which is switched off at time τ_1 and on again at time τ_2, and an initially Gaussian probe

$$V_p(t,z=0) = V_p(t=0,z=0)\exp\left[-(t-t_p)^2/\tau_p^2\right], \quad (18)$$

centered at time t_p with width τ_p. The propagation of the control field and probe pulse are determined by the propagation equations

$$\left(\frac{d}{dz}+\frac{1}{c}\frac{d}{dt}\right)V_c = i\alpha\left(\rho_{31}'^{(0)}+\rho_{32}'^{(0)}\right), \quad (19)$$

$$\left(\frac{d}{dz}+\frac{1}{c}\frac{d}{dt}\right)V_p = i\alpha\left(\rho_{31}'^{(1)}+\rho_{32}'^{(1)}+\rho_{31}'^{(-1)}+\rho_{32}'^{(-1)}\right), \quad (20)$$

where $\mathrm{Im}\rho_{31,32}'^{(-1)}$ is proportional to the absorption of the field generated at the FWM frequencies $\omega_{\mathrm{FWM}} = 2\omega_c - \omega_p$, which are the same as the two-photon resonance frequencies (if $\omega_p = \omega_c \pm 2\Delta_z$ and $\omega_{\mathrm{FWM}} = \omega_c \mp 2\Delta_z$) and α is proportional to the unsaturated absorption coefficient.

III. RESULTS AND DISCUSSION

We begin by solving the steady-state matrix equation (11) for the system depicted in Fig. 1 for both the cases where the control and probe fields have parallel linear polarizations (lin ∥ lin) and where they have perpendicular polarizations (lin ⊥ lin). We discuss the probe absorption spectrum along with the coherent population oscillations $\rho_{11}^{(1)}$ and $\rho_{22}^{(1)}$ and the two-photon coherence $\rho_{21}^{(1)}$. We then proceed to solve the propagation equations (19) and (20) and show how the temporal shape of the retrieved probe is related to the time dependence of the coherent population oscillations and the two-photon coherence. We note that all the parameters are normalized by $\Gamma = \Gamma_{31} = \Gamma_{32}$. In all the cases we consider, the probe is assumed to be much weaker than the control field so that it is sufficient to take $n_{\max} = 2$.

A. Probe absorption spectrum

The probe absorption spectra are shown in Fig. 2 for the case where a longitudinal magnetic field raises the degeneracy of the Zeeman sublevels so that $\Delta_{31} = -\Delta_{32} = 1$. In the top panel, the probe absorption spectrum is shown for parallel pump and probe polarizations (lin ∥ lin) and, in the bottom panel, for perpendicular pump and probe polarizations (lin ⊥ lin). In each case, we compare an open system where $\gamma_{3t} > \gamma_t$ with a closed system where $\gamma_{3t} = \gamma_t$. As expected, the spectra for the open system are much weaker than those for the closed system. All four spectra in Fig. 2 are characterized by two EIT dips at the two-photon resonances $\delta = \pm 2\Delta_{31}$. These originate from the two-photon resonant Λ systems formed by the interaction of a σ^+ pump (probe) with the $|1\rangle \rightarrow |3\rangle$ transition and σ^- probe (pump) with the $|2\rangle \rightarrow |3\rangle$ transition. The spectral features at line center $\delta = 0$ arise as a result of the interaction of σ^+ pump and probe with the $|1\rangle \rightarrow |3\rangle$ transition and σ^- pump and probe with the $|2\rangle \rightarrow |3\rangle$ transition. For the closed system, a CPO dip appears at line center for perpendicular polarizations but does not appear in the case of parallel polarizations. The lack of a dip at line center for the closed system is in line with earlier work on this system [24,27,28], which only considered lin ∥ lin polarized fields interacting with a closed system. For the open system, CPO dips appear for both parallel and perpendicular polarizations [29] but the dip is much narrower in the lin ∥ lin case. The case of parallel polarizations in the Λ system considered here can be compared to the open TLS for the same parameters [9,10] where the width of the dip is determined by γ_t. In the case of the perpendicular polarizations, we can see from Fig. 2 that the widths of the EIT and CPO dips are similar. We have not introduced phase-changing collisions or Doppler broadening in our calculations. In general, these broadening mechanisms do not affect the width of the narrow spectral features [9]. In Sec. III A, we will compare the storage of a probe pulse with frequency equal to that of the pump for parallel and perpendicular polarizations for both the nondegenerate system (Fig. 2) and the degenerate system (Fig. 3).

In Fig. 3, we show the probe absorption spectra for the same cases as in Fig. 2 but for the situation where the ground Rabi sublevels are degenerate as would occur in the absence of a

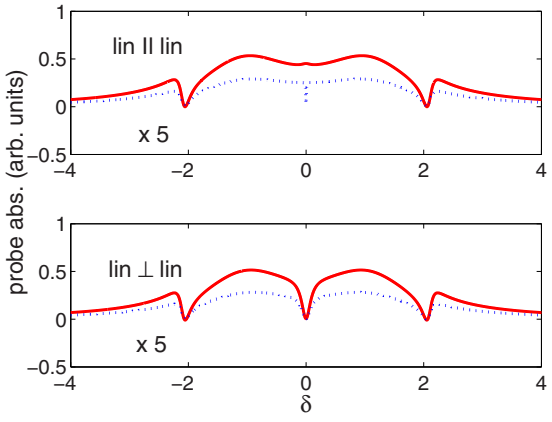

FIG. 2. Probe absorption spectrum as a function of pump-probe detuning for $F_g = 1 \rightarrow F_e = 1$ transition in the presence of longitudinal magnetic field for lin ∥ lin and lin ⊥ lin polarizations. The quantity plotted is $\mathrm{Im}(\rho_{31}'^{(1)}/V_p + \rho_{32}'^{(1)}/rV_p)$, which is proportional to the probe absorption [26]. The parameters used are $|V_c| = 0.3$, $|V_p| = 0.001$, $\Delta_{31} = -\Delta_{32} = 1$, $\gamma_{21} = \gamma_{12} = \gamma_t$, $\gamma_t = 0.001$, $\gamma^* = 0$, and $\gamma_{3t} = 0.001$ (closed system, solid red line) and $\gamma_{3t} = 0.2$ (open system, dotted blue line). The plot for the open system is magnified fivefold. All the parameters are normalized by the population decay rate $\Gamma = \Gamma_{31} = \Gamma_{32}$ and are thus dimensionless.

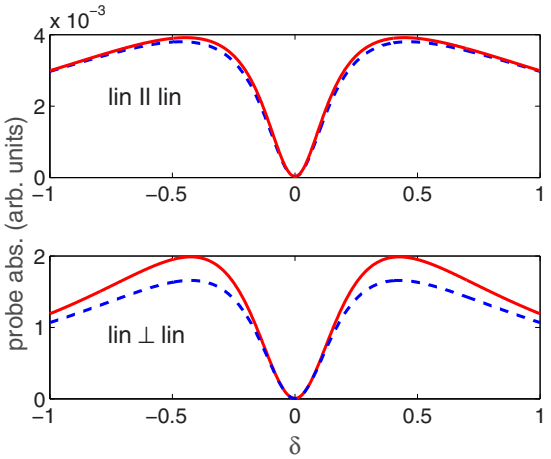

FIG. 3. Probe absorption spectrum as a function of pump-probe detuning for $F_g = 1 \rightarrow F_e = 1$ transition in the absence of longitudinal magnetic field for lin ∥ lin and lin ⊥ lin polarizations. The quantity plotted is $\mathrm{Im}(\rho_{31}^{\prime(1)}/V_p + \rho_{32}^{\prime(1)}/rV_p)$, which is proportional to the probe absorption [26]. The parameters used are $|V_c| = 0.3$, $|V_p| = 0.001$, $\Delta_{31} = -\Delta_{32} = 0$, $\gamma_{21} = \gamma_{12} = \gamma_t$, $\gamma_t = 0.001$, $\gamma^* = 0$, and $\gamma_{3t} = 0.001$ (closed system, solid red line) and $\gamma_{3t} = 0.2$ (open system, dotted blue line). All the parameters are normalized by Γ and are thus dimensionless.

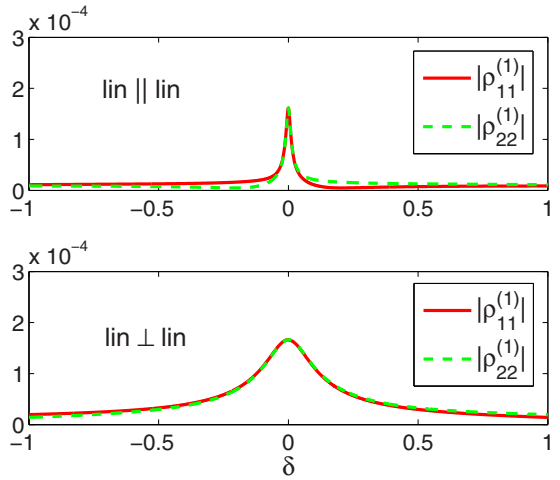

FIG. 4. Absolute values of the coherent population oscillations $\rho_{11}^{(1)}$ (full red line) and $\rho_{22}^{(1)}$ (dashed green line) as a function of pump-probe detuning for an open $F_g = 1 \rightarrow F_e = 1$ transition in the presence of longitudinal magnetic field for lin ∥ lin and lin ⊥ lin polarizations. The parameters used are $|V_c| = 0.3$, $|V_p| = 0.001$, $\Delta_{31} = -\Delta_{32} = 1$, $\gamma_t = 0.001$, $\gamma_{21} = \gamma_{12} = \gamma_t$, $\gamma^* = 0$, and $\gamma_{3t} = 0.2$. All the parameters are normalized by Γ and are thus dimensionless.

magnetic field, so that $\Delta_{31} = \Delta_{32} = 0$. Here, the CPO and EIT dips coincide at $\delta = 0$ and, as in the nondegenerate system, the dip is wider for the perpendicular case. However, in addition, the absorption is much stronger in the perpendicular case than in the parallel one. This will have important consequences when we consider the propagation of a probe pulse.

B. Coherent population oscillations and two-photon coherence

In Sec. III C, we will study the storage of a probe pulse in an attempt to determine which factors control whether its temporal shape will be restored. In order to clarify this issue, it is necessary to study the behavior of the steady-state coherent population oscillations and two-photon coherences near line center, in the presence and absence of a magnetic field.

In Fig. 4, we plot the absolute values of the coherent population oscillations $\rho_{11}^{(1)}$ and $\rho_{22}^{(1)}$ near line center for parallel polarizations (upper panel) and perpendicular polarizations (lower panel) for the same parameters as Fig. 2 for an open system with $\gamma_{3t} = 0.2$. The widths of the peaks are in accord with those of the probe absorption spectra at line center, namely, wider for the perpendicular polarizations. For the case where $\Delta_{31} = -\Delta_{32} = -1$, the CPOs $\rho_{11}^{(1)}$ and $\rho_{22}^{(1)}$ would be interchanged. The absolute values of the coherent population oscillations are depicted in Fig. 5 for the same parameters as in Fig. 3 for $\gamma_{3t} = 0.2$. Here we see that, in contrast to the nondegenerate case of Fig. 3, here the populations for the perpendicular case are much larger than those for the parallel case. This is reflected in the greater probe absorption for the perpendicular case, as depicted in Fig. 3. In Figs. 4 and 5, we plotted the absolute values of the CPOs. If we consider the real and imaginary parts of the CPOs, we find that $\rho_{11}^{(1)}$ and $\rho_{22}^{(1)}$ have the same phase for the parallel case but opposite phases for the perpendicular case ($\rho_{11}^{(1)} = -\rho_{22}^{(1)}$) as shown previously [29].

In Fig. 6, we show the two-photon coherence oscillations $\rho_{21}^{(1)}$ and $\rho_{21}^{(-1)}$ for the nondegenerate system with the same parameters as in Fig. 4. We see that the two-photon coherences have peaks at the appropriate two-photon resonances but are very small at line center in contrast to the CPOs which have

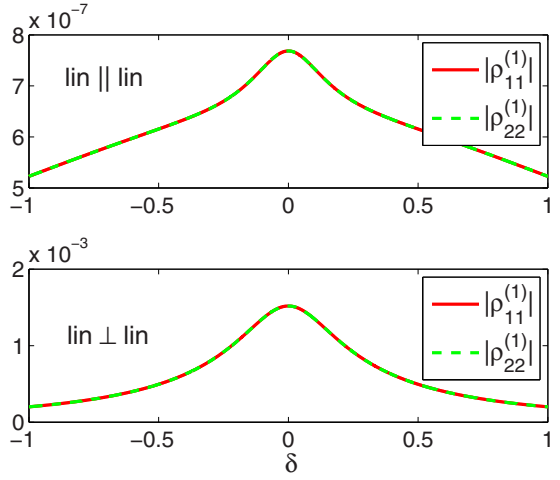

FIG. 5. Absolute values of the coherent population oscillations $\rho_{11}^{(1)}$ (full red line) and $\rho_{22}^{(1)}$ (dashed green line) as a function of pump-probe detuning for an open $F_g = 1 \rightarrow F_e = 1$ transition in the absence of longitudinal magnetic field for lin ∥ lin and lin ⊥ lin polarizations. The parameters used are $|V_c| = 0.3$, $|V_p| = 0.001$, $\Delta_{31} = -\Delta_{32} = 0$, $\gamma_t = 0.001$, $\gamma_{21} = \gamma_{12} = \gamma_t$, $\gamma^* = 0$, and $\gamma_{3t} = 0.2$. All the parameters are normalized by Γ and are thus dimensionless.

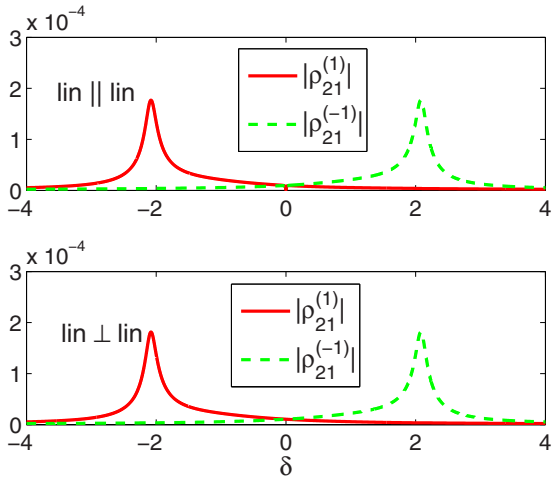

FIG. 6. Two-photon coherences $\rho_{21}^{(1)}$ (full red line) and $\rho_{21}^{(-1)}$ (dashed green line) as a function of pump-probe detuning for $F_g = 1 \rightarrow F_e = 1$ transition in the presence of longitudinal magnetic field for lin ∥ lin and lin ⊥ lin polarizations. The parameters used are $|V_c| = 0.3, |V_p| = 0.001, \Delta_{31} = -\Delta_{32} = 1, \gamma_t = 0.001, \gamma_{21} = \gamma_{12} = \gamma_t, \gamma^* = 0$, and $\gamma_{3t} = 0.2$. All the parameters are normalized by Γ and are thus dimensionless.

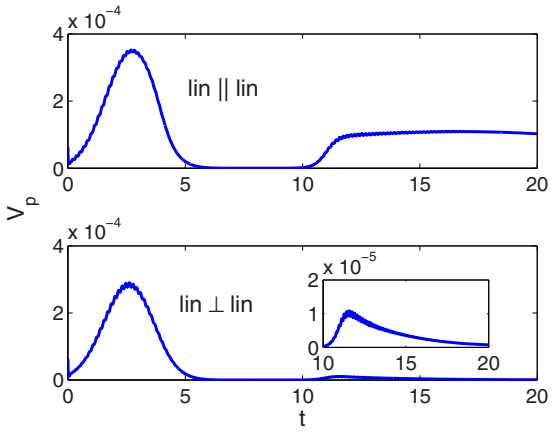

FIG. 8. Probe amplitude as a function of time for $z = 3 \times 10^{-4}$ at line center ($\delta = 0$) for $F_g = 1 \rightarrow F_e = 1$ transition in the presence of longitudinal magnetic field for lin ∥ lin and lin ⊥ lin polarizations (the inset contains a magnified version of the restored probe). The parameters used are $|V_c(t = 0, z = 0)| = 0.3$, $|V_p(t = 0, z = 0)| = 0.001$, $\Delta_{31} = -\Delta_{32} = 1$, $\gamma_{3t} = 0.2$, $\gamma_t = 0.001$, $\gamma_{21} = \gamma_{12} = \gamma_t$, $\gamma^* = 0$, $t_p = 2.5, \tau_p = 1.5, \tau_1 = 4, \tau_2 = 11$, and $\alpha = 10^4$. All the parameters are normalized by Γ and are thus dimensionless.

peaks at line center. In Fig. 7, we show the two-photon coherence oscillations for the degenerate case (same parameters as Fig. 5). The coherence oscillations for the perpendicular case are larger than for the parallel case. This is in agreement with the behavior of the population oscillations (see Fig. 5).

The value of $\rho_{21}^{(0)}$, the two-photon coherence which derives from the interaction of the $\sigma^{(+)}$ component of the pump interacting with the $|1\rangle \rightarrow |3\rangle$ transition and its $\sigma^{(-)}$ component interacting with the $|2\rangle \rightarrow |3\rangle$ transition, can be calculated for the nondegenerate and degenerate configurations. For the nondegenerate case, $\rho_{21}^{(0)} = 0.002 + 0.0024i$, whereas for the degenerate case, $\rho_{21}^{(0)} = -0.46$, which is close to the maximum coherence value of -0.5.

In the next section, we discuss probe propagation for both the nondegenerate and degenerate cases and show that the temporal shape of the restored probe is only restored for the degenerate case.

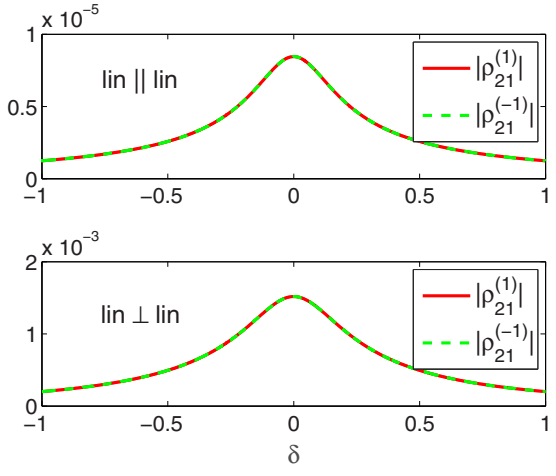

FIG. 7. Two-photon coherences $\rho_{21}^{(1)}$ (full red line) and $\rho_{21}^{(-1)}$ (dashed green line) as a function of pump-probe detuning for $F_g = 1 \rightarrow F_e = 1$ transition in the absence of longitudinal magnetic field for lin ∥ lin and lin ⊥ lin polarizations. The parameters used are $|V_c| = 0.3, |V_p| = 0.001, \Delta_{31} = -\Delta_{32} = 0, \gamma_t = 0.001, \gamma_{21} = \gamma_{12} = \gamma_t, \gamma^* = 0$, and $\gamma_{3t} = 0.2$. All the parameters are normalized by Γ and are thus dimensionless.

C. Probe propagation

In this section, we study the storage of a probe pulse whose frequency is equal to that of the pump field $\delta = 0$ when the pump field is switched off and then on again. We compare the nondegenerate case (see Fig. 2) where the EIT dips flank the central CPO dip (see Fig. 2) and the degenerate case where all three dips coincide. For both cases, we plot the probe absorption at line center for a probe pulse that is initially centered at $t = t_p = 1.5$ with width $\tau_p = 2.5$ and a control field that is switched off at $t = \tau_1 = 4$ and on again at $t = \tau_2 = 11$. For the nondegenerate case shown in Fig. 8, we consider the time dependence of the probe on propagation for a value of z where the amplitude of the restored pulse is significant. For the degenerate case shown in Fig. 9, the probe propagation is displayed as a function of z and t. The main difference between Figs. 8 and 9 lies in the shape of restored pulse: for the degenerate case, the restored pulse has the same general shape as the initial pulse, whereas for the nondegenerate case, the restored pulse is smeared, similar to the behavior obtained for a two-level system with shelving state [2]. This lack of well-defined temporal shape has been observed experimentally in light-storage experiments performed on metastable He [3,16] and Cs [4] atomic vapor where the pump and signal fields have orthogonal linear polarizations and a longitudinal magnetic field is applied.

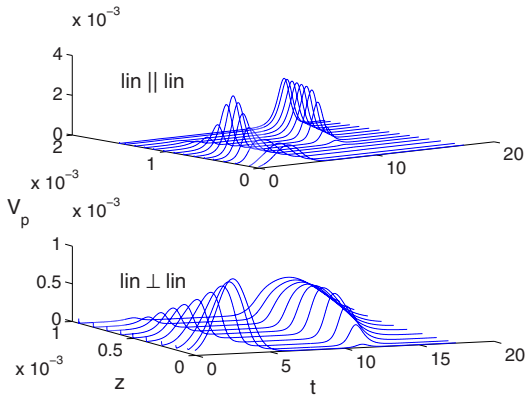

FIG. 9. Probe amplitude as a function of time for various propagation distances at line center ($\delta = 0$) for $F_g = 1 \rightarrow F_e = 1$ transition in the absence of longitudinal magnetic field for lin ∥ lin and lin ⊥ lin polarizations. The parameters used are $|V_c(t = 0, z = 0)| = 0.3$, $|V_p(0, z = 0)| = 0.001$, $\gamma_t = 0.001$, $\gamma_{21} = \gamma_{12} = \gamma_t$, $\Delta_{31} = \Delta_{32} = 0$, $\gamma_{3t} = 0.2$, $\gamma^* = 0$, $t_p = 2.5$, $\tau_p = 1.5$, $\tau_1 = 4$, $\tau_2 = 11$, and $\alpha = 10^4$. All the parameters are normalized by Γ and are thus dimensionless.

In order to understand the difference between the degenerate and nondegenerate cases, it is advisable to refer to the behavior of the coherent population oscillations and two-photon coherence oscillations shown in Figs. 4– 7. For the nondegenerate case, we see that the CPOs are much greater than the coherence oscillations at line center (compare Figs. 4 and 6) whereas, in the degenerate case, the two-photon coherence oscillations at line center are an order of magnitude greater than the CPOs for parallel polarizations and of the same order of magnitude for perpendicular polarizations (compare Figs. 5 and 7). Thus the CPOs determine the lack of the shape of the restored probe pulse in the nondegenerate case, whereas the two-photon coherence oscillations contribute to the temporal shape of the restored pulse in the degenerate case, similar to the behavior observed in EIT experiments where the two-photon coherence oscillations remember the shape of the incident probe pulse [15,30,31]. The difference in behavior of the initial probe pulse on propagation between the two polarization schemes shown in Fig. 9 can be explained by considering the difference in the probe absorption spectra shown in Fig. 3. There we see that the absorption is much greater for the case of perpendicular polarizations so that the pulse is absorbed on propagation. This absorption could be mitigated by considering a longer probe pulse which would have a narrower spectral bandwidth.

IV. CONCLUSIONS

We have considered the $F_g = 1 \rightarrow F_e = 1$ transition between the ground and excited hyperfine levels in alkali-metal vapor interacting with σ linearly polarized control and probe fields whose polarizations can be either parallel or perpendicular to each other. We developed a matrix formulation that allows a solution of the Bloch equations to all orders in the pump and probe Rabi frequencies. Using this formalism, we calculated the steady-state probe absorption spectrum, the coherent population oscillations (CPOs), and two-photon coherence oscillations, in the absence (degenerate case) and presence (nondegenerate case) of a longitudinal magnetic field. We then calculated the probe storage when the pump is switched off and on again. We were particularly interested in whether the probe regains its original temporal shape when the pump is switched on again for the case where the control-probe frequency difference is zero as the CPO dip is centered at this point. We showed that, in the nondegenerate case, the restored probe does not regain its original shape whereas, in the degenerate case, the original shape is restored. This can be explained by considering the relative magnitudes of the CPOs which do not remember the temporal shape of the probe, as we showed for the case of a two-level system with shelving state [2] and the two-photon coherence which stores the pulse shape when the pump is switched off, as in electromagnetically induced transparency (EIT) memories [32]. In the nondegenerate case, the CPOs are much stronger than the coherence oscillations whereas, in the degenerate case, they are of similar magnitudes. Thus it is the two-photon coherence oscillations that are responsible for the restoration of the temporal shape of the probe in the degenerate case.

The degenerate system is simultaneously a double-EIT system (control and probe fields on different legs) [31] and a double-coherent-population-trapping (CPT) system (control and probe fields on the same leg) [33]. The restoration of the pulse shape is due to the contribution of the double-EIT system, which is an extension of the single-EIT system [32] and has some features in common with pulse storage in an amplifying double-Λ system [30]. It should be pointed out that, although storage of the temporal pulse shape cannot be achieved by CPO alone, one can still obtain storage of its spatial shape as proposed for the TLS that decays via a metastable state [2].

[1] K. Hammerer, A. S. Sorensen, and E. S. Polzik, Rev. Mod. Phys. **82**, 1041 (2010).
[2] A. Eilam, I. Azuri, A. V. Sharypov, A. D. Wilson-Gordon, and H. Friedmann, Opt. Lett. **35**, 772 (2010).
[3] M.-A. Maynard, F. Bretenaker, and F. Goldfarb, Phys. Rev. A **90**, 061801 (2014).
[4] A. J. F. de Almeida, J. Sales, M.-A. Maynard, T. Lauprêtre, F. Bretenaker, D. Felinto, F. Goldfarb, and J. W. R. Tabosa, Phys. Rev. A **90**, 043803 (2014).
[5] M. Sargent III, Phys. Rep. **43**, 223 (1978).
[6] R. W. Boyd, M. G. Raymer, P. Narum, and D. J. Harter, Phys. Rev. A **24**, 411 (1981).
[7] G. Khitrova, P. R. Berman, and M. Sargent, J. Opt. Soc. B **5**, 160 (1988).
[8] H. Friedmann, A. D. Wilson-Gordon, and M. Rosenbluh, Phys. Rev. A **33**, 1783 (1986).
[9] A. D. Wilson-Gordon and H. Friedmann, Opt. Lett. **14**, 390 (1989).
[10] S. Hochman, A. D. Wilson-Gordon, and H. Friedmann, Opt. Lett. **15**, 631 (1990).

[11] S. E. Schwarz and T. Y. Tan, Appl. Phys. Lett. **10**, 4 (1967).
[12] R. W. Boyd and D. J. Gauthier, in *Progress in Optics*, edited by E. Wolf (Elsevier, Amsterdam, 2002), Vol. 43, Chap. 6.
[13] A. V. Sharypov, A. Eilam, A. D. Wilson-Gordon, and H. Friedmann, Phys. Rev. A **81**, 013829 (2010).
[14] I. Azuri, A. Eilam, A. V. Sharypov, A. D. Wilson-Gordon, and H. Friedmann, Opt. Commun. **283**, 4318 (2010).
[15] M. Fleischhauer and M. D. Lukin, Phys. Rev. A **65**, 022314 (2002).
[16] P. Neveu, M.-A. Maynard, R. Bouchez, J. Lugani, R. Ghosh, F. Bretenaker, F. Goldfarb, and E. Brion, Phys. Rev. Lett. **118**, 073605 (2017).
[17] A. J. F. de Almeida, S. Barreiro, W. S. Martins, R. A. de Oliveira, D. Felinto, L. Pruvost, and J. W. R. Tabosa, Opt. Lett. **40**, 2545 (2015).
[18] R. A. de Oliveira, G. C. Borba, W. S. Martins, S. Barreiro, D. Felinto, and J. W. R. Tabosa, Opt. Lett. **40**, 4939 (2015).
[19] D. Moretti, D. Felinto, and J. W. R. Tabosa, Phys. Rev. A **79**, 023825 (2009).
[20] A. Nicolas, L. Veissier, L. Giner, E. Giacobino, D. Maxein, and J. Laurat, Nat. Photon. **8**, 234 (2014).
[21] C. Goren, A. D. Wilson-Gordon, M. Rosenbluh, and H. Friedmann, Phys. Rev. A **67**, 033807 (2003).
[22] M. V. Pack, R. M. Camacho, and J. C. Howell, Phys. Rev. A **76**, 013801 (2007).
[23] S. Boublil, A. D. Wilson-Gordon, and H. Friedmann, J. Mod. Opt. **38**, 1739 (1991).
[24] A. D. Wilson-Gordon, Phys. Rev. A **48**, 4639 (1993).
[25] M. Auzinsh, D. Budker, and S. M. Rochester, *Optically Polarized Atoms* (Oxford University Press, Oxford, 2010).
[26] C. Goren, A. D. Wilson-Gordon, M. Rosenbluh, and H. Friedmann, Phys. Rev. A **68**, 043818 (2003).
[27] S. Menon and G. S. Agarwal, Phys. Rev. A **59**, 740 (1999).
[28] A. D. Wilson-Gordon and H. Friedmann, J. Mod. Opt. **49**, 125 (2002).
[29] T. Lauprêtre, S. Kumar, P. Berger, R. Faoro, R. Ghosh, F. Bretenaker, and F. Goldfarb, Phys. Rev. A **85**, 051805(R) (2012).
[30] A. Eilam, A. D. Wilson-Gordon, and H. Friedmann, Opt. Lett. **33**, 1605 (2008).
[31] A. Eilam, A. D. Wilson-Gordon, and H. Friedmann, Opt. Lett. **34**, 1834 (2009).
[32] M. Fleischhauer, A. Imamoglu, and J. P. Marangos, Rev. Mod. Phys. **77**, 633 (2005).
[33] A. Eilam, A. D. Wilson-Gordon, and H. Friedmann, Opt. Commun. **277**, 186 (2007).